Dual Graded Index Dielectric Lens System for Hyperthermia

Fernando Albarracin-Vargas*(1), Felix Vega(1)(2), Chaouki Kasmi(1)(3), Fahad AlYafei(1), and Christoph Baer(4)
(1) Directed Energy Research Centre, Technology Innovation Institute, Abu Dhabi, United Arab Emirates, https://tii.ae
(2) Universidad Nacional de Colombia - Sede Bogotá, Bogotá, Colombia
(3) Faculty of Electrical Engineering, Helmut Schmidt University, Hamburg, Germany
(4) Ruhr-University of Bochum, Bochum, Germany

Abstract

This paper presents a novel design for a microwave applicator for hyperthermia applications, based on the combination of two flat dielectric graded-index (GRIN) lenses. The proposed system is a suitable alternative to conventional antenna-based applicators. The presented approach considers the interface between free-space and-tissue, an aspect that has been disregarded by the conventional microwave applicators reported so far.

1 Introduction

Hyperthermia is a technique that has gain increasing attention in the biomedical community as a complementary treatment of cancer [1], [2]. External hyperthermia is the non-invasive alternative of increasing the temperature of the target tissue by electromagnetic or ultrasound radiation into the affected area [1]. In the treatment of cancer with external hyperthermia, it is desirable to apply the radiation in a localized point into the body. Tumors are heated by exposure to the radiation up to temperatures of 41° to 43° [2].

The need for focusing a certain amount of energy into a specific area involves the study of the phenomena of propagation of electromagnetic waves within non-homogeneous and lossy media [1]. The amount of heat that is induced in tissues when radiated by microwaves systems is related to the Specific Absorption Rate, SAR, in (W/kg), or by the Power Loss Density, PLD, in (W/m^3) [1].

Most of the external hyperthermia techniques reported so far involve the use of microwave applicators, without considering the transition between the free space and the tissue [3]–[6]. Since the human body is known as a very lossy media with high electric permittivity, due to its high-water content level, the transition of a traveling wave in the boundary air-tissue must be considered.

Dielectric graded refractive index, GRIN, lenses applied to transient ultra-wideband radiating systems, was proposed by Baum in [7]. These are an easy-to-implement alternative to build a focused external hyperthermia applicator. This technique allows fabricating flat and thin dielectric lenses in the microwave regime, as reported in [8], [9], [10].

2 Single Lens Design

The zero-phase difference analysis consists of equating the phase difference between the ray-path connecting the incident plane wave to the focal point, *F,* at angles $\alpha \neq 0$ (see Figure 1 as a reference), to the resulting phase of the axial ray-path (i.e., for $\alpha = 0$). Zero-phase difference analysis is described in (1) through (5), by calculating the travel time for each stage comprising the ray-path. Then, for each possible ray-path from a plane, orthogonal to the lens' axis, containing the incident plane wave-front, there will be a specific transit time upon a point, the focal point, on the opposite side. Thus, the transit time through the lens is gradually reduced by decreasing the permittivity value of the material as the ray-path reaches the lens outer edge, enabling the implementation of a convergent spherical wave in the right-side of the dielectric GRIN lens.

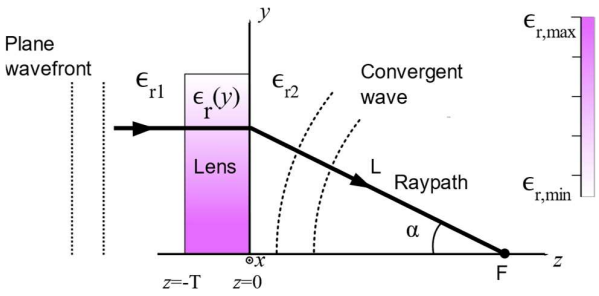

Figure 1. Sketch of the zero-phase difference approach.

Figure 1 depicts the sagittal plane of the upper half of and presents the reference axis and angles involved in the analysis.

The zero phase difference requires equal transit time for the rays traveling on and off-axis. This is stated in (1) where the equivalent travel distance is introduced. On the left side of the equation we present the equivalent travel distance for an on axis rays, i.e. $\alpha = 0°$, (the shortest path to the target). The right side describes the equivalent travel distance for off axis trajectories i.e. $\alpha \neq 0°$. For the description of the analysis, we will consider the case when the lens is surrounded by free space (i.e., $\varepsilon_{r1} = \varepsilon_{r2} = 1$).

$$F \cdot \sqrt{\varepsilon_{r2}} + T \cdot \sqrt{\varepsilon_{r\max}} = L \cdot \sqrt{\varepsilon_{r2}} + T \cdot \sqrt{\varepsilon_r(y)}, \qquad (1)$$

where T is the lens thickness, $\varepsilon_{r1} = \varepsilon_{r2} = 1$ is the free space relative permittivity, and $\varepsilon_{r,max} = \varepsilon_r(y = 0)$. Since:

$$L = F / \cos(\alpha), \tag{2}$$

we can replace (2) into (1):

$$F \cdot \sqrt{\varepsilon_{r2}} + T \cdot \sqrt{\varepsilon_{r,\max}} = \left(\frac{F}{\cos(\alpha)} \right) \cdot \sqrt{\varepsilon_{r2}} + T \cdot \sqrt{\varepsilon_r(y)}. \tag{3}$$

Solving for $\varepsilon_{r,y}$ we have:

$$\varepsilon_r(y) = \left(\frac{F}{T} \cdot \left(1 - \frac{1}{\cos(\alpha)} \right) + \cdot \sqrt{\varepsilon_{r,\max}} \right)^2. \tag{4}$$

The higher the permittivity value at the center of the lens is, the thinner the lens width is, reducing the overall lens weight. On the other hand, the permittivity of the outer ring should be as close as possible to 1 to reduce the diffraction effect at the lens edge.

In the remaining of this work, the media where the convergent spherical wave propagates will be lossy and will present a relative permittivity higher than that from the free space. The measured values of losses and relative permittivity of different types of tissues are presented in [1], [5].

2.1 Refractive Index Discretization

One of the most challenging tasks in the fabrication of a GRIN lens is the implementation of the intended electrical permittivity. Even though the increasing availability of 3D-printers and the sophisticated Computer-Aided Design (CAD) software for controlling such printing hardware, the implementation of material with a specific spatial-dependent permittivity continuous function (e.g., $\varepsilon_r(y)$) have to be discretized in some way, as described in [9], [10]. For this reason, it is necessary to discretize the permittivity of the lens material as a function of the radial distance from its axis, dividing the structure into several rings. The resulting number of rings can be named as the discretization factor, n.

Due to the axial symmetry in a cylindrical lens, the radial distance from the lens axis is simplified to the rectangular coordinate, y, in this analysis. However, the resulting convergent wave is spherical. For implementing the discrete permittivity values, the so-called RF-design materials, as proposed in [11], can be utilized. These composites consist of a host low permittivity material (e.g., silicon pottant) doped by a precise volumetric concentration of a low-loss high-permittivity material in the form of powder. The process of synthesizing the resultant material involves a temperature-controlled curation stage, as described in [11]. The permittivity values that have been obtained with this technique range from 2 to 10, with a loss tangent $\tan(\delta) \leq 0.08$.

Figure 2 shows the discretization of the radial function of permittivity, $\varepsilon_r(y)$, by computing a sequence of stepwise function whose amplitude represents the permittivity of uniform dielectric rings. Each one of such a set of rings has a fixed permittivity value equal to the central-point-crossing value with the continuous function in (4) (i.e., blue curve in Figure 2). Thus, a number n of coaxial and concentric dielectric rings are placed to form the complete lens' structure.

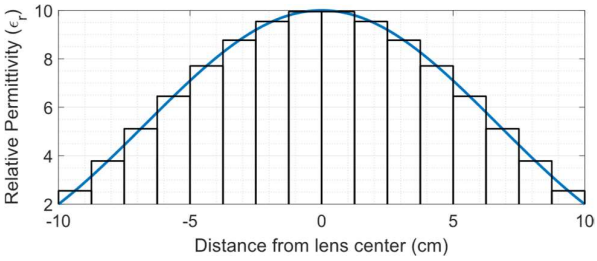

Figure 2. Radial variation of the relative permittivity from the center of the lens, and its discretization in n = 8 rings, shown as a stepwise function.

3 Dual Lens System

To control the effective location of the focal point of the electromagnetic radiation inside the tissue, a dual-lens system is proposed. The system will consist of two flat GRIN lenses separated by a distance, d, see Figure 3 for reference. The plane wave produced by a microwave source will enter into Lens-2 and will be converted into a convergent spherical wave, whose focal length is larger than the distance separating the two lenses. Then, the convergent spherical wave is converted again into a more-convergent wave, with an effective focal length shorter than that from both lenses. Finally, by changing the separation between the lenses, the effective focal point, F_{eff}, can be controlled. F_{eff} can be understood as the point at which constructive interference will increase the volumetric power density in the target tissue.

Figure 3 shows the dual GRIN lens approach where F_1 and F_2 are the focal lengths from Lens-1 and Lens-2, respectively. The radial axis of both lenses is aligned along the z-axis, as well as their focal points.

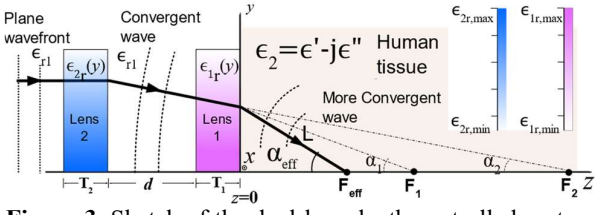

Figure 3. Sketch of the dual-lens depth controlled system approach.

As mentioned above, the losses must be considered in the analysis of the travel time inside the tissue. Since the losses can be accounted for by including the loss tangent parameter, tan*(δ),* the permittivity expression is

$$\varepsilon_2 = \varepsilon' - j\varepsilon'' = \varepsilon'(1 - j\tan(\delta)) \quad (5)$$

where tan*(δ)* = ε"/ ε', and ε' = $\varepsilon_0\varepsilon_{r2}$. tan*(δ)* accounts for both the losses due to the damping of electrical dipole moments in the tissue and for its conductivity (i.e., ohmic losses). The parameter ε" can be approximated as [1]

$$\varepsilon'' = \frac{\sigma}{\omega\varepsilon_0} \quad (5)$$

where ω is the angular frequency in (rad/s), and σ the conductivity in (Sm^{-1}). Then, the propagation constant inside the lossy medium, k_2, is

$$k_2 = \omega\sqrt{\mu_2\varepsilon_2} = \omega\sqrt{\mu_0\varepsilon'}\sqrt{(1 - j\tan(\delta))} = \beta - j\alpha. \quad (6)$$

where β is the phase constant in (rad/m), and α is the attenuation factor in (Neper/m). By taking the first values of the approximation

$$(1+x)^{1/2} = 1 + \frac{1}{2}x - \frac{1}{8}x^2 \ldots \quad (7)$$

the propagation constant in (6) can be re-written as

$$k_2 = \beta - j\alpha = \omega\sqrt{\mu_0\varepsilon_0}\sqrt{\varepsilon_{r2}}\left(1 - \frac{1}{8}\tan^2\delta\right) - j\omega\sqrt{\mu_0\varepsilon_0}\sqrt{\varepsilon_{r2}}\left(\frac{1}{2}\tan\delta\right) \quad (8)$$

Thus, the propagation velocity in the lossy medium, v_{p2}= ω/ β can be computed as

$$v_{p2} = \frac{\omega}{\omega\sqrt{\mu_0\varepsilon_0}\sqrt{\varepsilon_{r2}}\left(1 - \frac{1}{8}\tan^2\delta\right)} = \frac{c}{\sqrt{\varepsilon_{r2}}\left(1 - \frac{1}{8}\tan^2\delta\right)} \quad (9)$$

Then, for the dual-lens configuration in Figure 3, the zero-phase difference analysis shall be carried out again. This time, including the travel time over the ray-path across the second lens, Lens-2, the space between the first and the second lens, *d*, and the correction due to the losses inside the tissue:

$$T_2\sqrt{\varepsilon_{2r}(y)} + \left(\frac{d+T_1}{\cos\alpha_{eff}}\right)\sqrt{\varepsilon_{r1}} + T_1\sqrt{\varepsilon_{1r}(y)} + \frac{F_{eff}}{\cos\alpha_{eff}}\sqrt{\varepsilon_{r2}}\left(1 - \frac{1}{8}\tan^2\delta\right) = T_2\sqrt{\varepsilon_{2r,\max}} + (d+T_1)\sqrt{\varepsilon_{r1}} + T_1\sqrt{\varepsilon_{1r,\max}} + F_{eff}\sqrt{\varepsilon_{r2}}\left(1 - \frac{1}{8}\tan^2\delta\right), \quad (10)$$

where $\varepsilon_{1r}(y)$ and $\varepsilon_{2r}(y)$ are computed as (11) and (12).

$$\varepsilon_{1r}(y) = \left(\frac{F_1}{T_1}\sqrt{\varepsilon_{r2}}\left(1 - \frac{1}{8}\tan^2\delta\right)\left(1 - \frac{1}{\cos(\alpha_1)}\right) + \sqrt{\varepsilon_{1r,\max}}\right)^2, \quad (11)$$

$$\varepsilon_{2r}(y) = \left(\frac{F_2}{T_2}\sqrt{\varepsilon_{r1}}\left(1 - \frac{1}{\cos(\alpha_2)}\right) + \sqrt{\varepsilon_{2r,\max}}\right)^2. \quad (12)$$

Each point of the ray-path, bent at Lens-2, is mapped upon a point in the Lens 1, with an incidence angle α_2, and bent again to converge to the effective focal point, $0 < F_{eff} < F_1$, along the *z*-axis.

Thus, F_1 shall be set to the deepest point inside the tissue under treatment. F_2 should be larger than F_1. This leads to a transition from a less convergent to a more convergent spherical wave. As *d* is increased, F_{eff} tends to zero at $z = 0$ (the Lens-Tissue boundary in Figure 3). The maximum lens separation can be ideally computed as the value of *d,* in (10), that gives a $F_{eff} = 0$, for the maximum values of α_1 and α_2.

3.1 Design Example

It has been shown in [4], [5] that at frequencies in the ISM 2.4 GHz band, a significant thermal exposure of malignant tissue is observed at 2-4 cm depth. A dual-lens system for a plane-wave source, working at 2.45 GHz is presented as a design example. For Lens-1, a diameter D = 20 cm is selected, F_1 is set to 15 cm. Permittivity values range from 2 to 10, according to the fabrication technique described above.

For the tissue values, a conductivity of 0.19 (S/m) and a relative permittivity of 10 are used for computing the travel time in this design. These values are those of a homogeneous healthy breast phantom presented in [4, Table 1]. By including these values in Equation (11), a thickness T_1= 4.32 cm can be obtained. Lens-2 is 40 cm in diameter, the same permittivity interval, and a focal length of cm. T_2 can be solved from (11) to be 1.59 cm. F_2= $2F_1$. The discretization factor, *n,* is set to 8 in both cases, giving a ring width of 1.25 cm and 2.5 cm, for Lens-1 and Lens-2, respectively. These are feasible dimensions, considering the fabrication technique. Figure 4 depicts the proposed convergent dual-lens configuration.

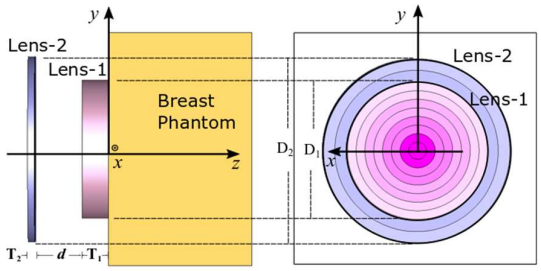

(a) (b)

Figure 4. Sketch of the dual-lens depth-controlled system. (a) Side view and (b) front view.

4 Results and Conclusion

A CAD model of the dual-lens system has been simulated in a full-wave electromagnetic simulator. Figure 5a shows the normalized PLD, along the *z*-axis inside the tissue (see Figure 4), for different lens separations, *d*. Figure 5b shows a 2D distribution of the power density for *d*=5 cm.

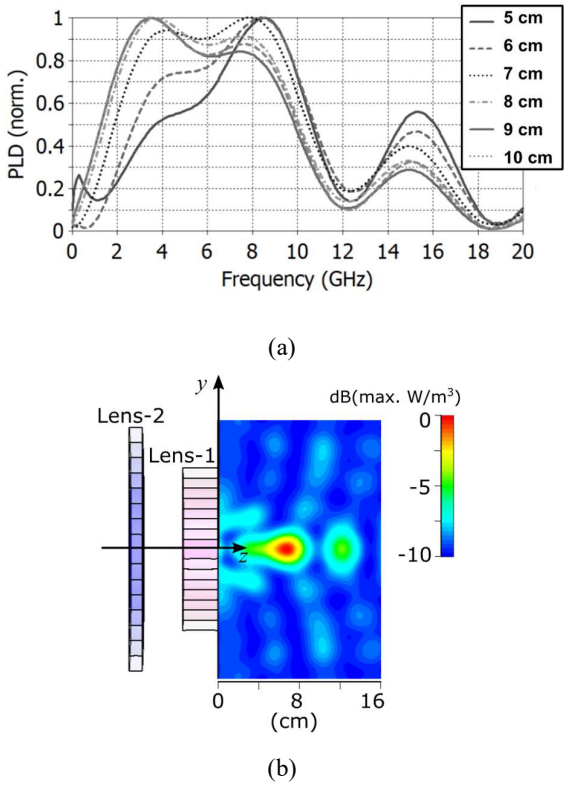

Figure 5. (a) Normalized PLD along the *z*-axis for a convergent dual-lens system for different lens separation, *d*. (b) 2D PLD distribution for *d* =5 cm.

The maximum PLD values were found in localized areas along the z-axis. This result confirms the focalization capability of the proposed design. The range of focusing is limited by the losses associated with the modeled tissue. Note that the PLD values were computed over a homogeneous healthy tissue model, with constant σ within the volume. No high conductivity material was included, as typically used to compute PLD over malignant tissue. Then, peak values of PLD can be expected when high conductivity malignant tissue models are introduced, and the lens system is focused over them.

A novel design of a focalized convergent-wave dielectric applicator for external hyperthermia treatment has been presented. The proposed system relies on a simple, feasible, and still effective technique for a localized thermal increase. Unlike most of the external antenna-based applicators, the dual-lens design considers the effects of the losses associated with human tissues. Any additional tissue type can be included in the design process in the form of additional layers, previously characterized by the complex ε parameter. The fabrication technique of the GRIN lenses comprising the system has been implemented and tested for different applications. Fabrication and test of an implemented prototype are in process.

5 References

[1] M. Gautherie, *Methods of External Hyperthermic Heating*. Springer Science & Business Media, 2012.

[2] I. Toseroni, S. Ciampa, and M. Cavagnaro, "Human body models for validation studies of deep hyperthermia," *International Journal of RF and Microwave Computer-Aided Engineering*, vol. 28, no. 3, p. e21207, 2018, doi: 10.1002/mmce.21207.

[3] J. C. Lin and Y.-J. Wang, "Interstitial microwave antennas for thermal therapy," *International Journal of Hyperthermia*, vol. 3, no. 1, pp. 37–47, Jan. 1987, doi: 10.3109/02656738709140371.

[4] I. Merunka, O. Fiser, L. Vojackova, J. Vrba, and D. Vrba, "Utilization potential of balanced antipodal Vivaldi antenna for microwave hyperthermia treatment of breast cancer," in *The 8th European Conference on Antennas and Propagation (EuCAP 2014)*, 2014, pp. 706–710, doi: 10.1109/EuCAP.2014.6901857.

[5] H. F. Guarnizo Mendez, M. A. Polochè Arango, J. J. Pantoja Acosta, J. F. Coronel Rico, and J. S. Amaya Opayome, "Hyperthermia Study in Breast Cancer Treatment Using Three Applicators," in *Applied Computer Sciences in Engineering*, Cham, 2019, pp. 416–427, doi: 10.1007/978-3-030-31019-6_36.

[6] S. Kotchapradit, T. Thosdeekoraphat, S. Santalunai, and C. Thongsopa, "Improvement of Electric Field Focusing for Deep Hyperthermia in Breast Cancer Treatment by Using Microwave Dielectric Heating with Curved Plate Applicator," in *2018 Asia-Pacific Microwave Conference (APMC)*, 2018, pp. 1474–1476, doi: 10.23919/APMC.2018.8617166.

[7] C. E. Baum, "Uniform Isotropic Dielectric Equal-Time Lenses for Matching Combinations of Plane and Spherical Waves," *Sensor and Simulation Notes*, vol. 352, p. 37, 1992.

[8] F. Albarracin-Vargas, F. Vega, C. Baer, K. Orend, and T. Musch, "Design Considerations in a Graded Index Flat Dielectric Lens for an Impulse Radiating Antenna," in *XXXIV Symposium of the International Union of Radio Science, URSI 2019*, Atlanta GA., 2019.

[9] S. Zhang, R. K. Arya, S. Pandey, Y. Vardaxoglou, W. Whittow, and R. Mittra, "3D-printed planar graded index lenses," *IET Microwaves, Antennas & Propagation*, vol. 10, no. 13, pp. 1411–1419, Oct. 2016, doi: 10.1049/iet-map.2016.0013.

[10] C. Mateo-Segura, A. Dyke, H. Dyke, S. Haq, and Y. Hao, "Flat Luneburg Lens via Transformation Optics for Directive Antenna Applications," *IEEE Transactions on Antennas and Propagation*, vol. 62, no. 4, pp. 1945–1953, Apr. 2014, doi: 10.1109/TAP.2014.2302004.

[11] B. Hattenhorst, M. Mallach, C. Baer, T. Musch, J. Barowski, and I. Rolfes, "Dielectric phantom materials for broadband biomedical applications," in *2017 First IEEE MTT-S International Microwave Bio Conference (IMBIOC)*, 2017, pp. 1–4, doi: 10.1109/IMBIOC.2017.7965802.